ISSN 0742-0463, Journal of Volcanology and Seismology, 2013, Vol. 7, No. 2, pp. 170–183. © Pleiades Publishing, Ltd., 2013.
Original Russian Text © A.V. Kiryukhin, S.V. Shadrina, M.Yu. Puzankov, 2013, published in Vulkanologiya i Seismologiya, 2013, No. 2, pp. 90–104.

Modeling the Thermohydrogeochemical Conditions for the Generation of Productive Reservoirs in Volcanogenic Rocks

A. V. Kiryukhin[a], S. V. Shadrina[b], and M. Yu. Puzankov[a]

[a] *Institute of Volcanology and Seismology, Far East Branch, Russian Academy of Sciences, Petropavlovsk-Kamchatskii, 683006 Russia*

e-mail: AVKiryukhin2@mail.ru

[b] *TO SurgutNipiNeft' OAO SurgutNefteGaz, Tyumen', ul. R. Lyuksemburg 12, 625003 Russia*

Received April 12, 2012

Abstract—This paper considers the role of hydrothermal processes in the generation of porous and permeable reservoirs in volcanogenic rocks, their boundedness with low-permeability interfaces, and the accumulation of fluids of various origins and phase states in the reservoirs. The Rogozhnikovskii productive reservoir is an example of a volcanogenic oil reservoir in western Siberia, it is confined to fluid upflows that are marked by positive anomalies in temperature and pressure. The Mutnovskii productive reservoir is an example of a high-temperature two-phase (water + steam) reservoir in Kamchatka that is supplied with deep heat-carrier upflows that are also associated with positive anomalies in temperature and pressure. The iTOUGH2 inversion simulation is used to estimate the discharge of deep upflows and then to represent a possible mechanism for the evolution of permeability–porosity and self-sealing of such reservoirs that result from water–rock chemical interaction. These methods are applied to the Rogozhnikovskii and Mutnovskii reservoirs. Both of these scenarios demonstrate the possible generation of productive reservoirs by hydrothermal circulation and show a short-lived drop in pressure during the earlier phase (which favors the inflow of fluids into the reservoir) and self-sealing with low-permeability interfaces during the later phase of hydrothermal circulation (which favors long-term storage of fluids in reservoirs).

DOI: 10.1134/S0742046313020036

INTRODUCTION

One of the more essential problems in earth sciences is the mechanisms that are operative in the generation of productive reservoirs in basement rocks; the origin of such reservoirs is apparently intimately related to their hydrothermal history. One example is the Rogozhnikovskii oil reservoir that was recently identified in the western Siberian basement; this is a giant oil reservoir in Permian–Triassic (250 Ma) volcanogenic basement rocks (rhyolites and lavas) at depths of 2.5–2.8 km and at temperatures as high as 140°C [Korovina et al., 2009; Chirkov et al., 2011]. Another example of an oil field at depths of 3–5 km in pre-Cenozoic basement granite (the White Tiger, Vietnam) [Kireeva, 2010] shows that oil is trapped in fault zones that have been altered by hydrothermal chloride sodium flows during the earlier phase of evolution.

Studies in the generation of productive, high-temperature, hydrothermal reservoirs in different hydrogeological structures of recent volcanic areas were rather fully reported in the 2010 proceedings of the International Geothermal Congress and in numerous other publications [Kiryukhin et al., 2010a, 2010b]. The examples of the Pauzhetka and Mutnovskii geothermal fields in Kamchatka show that the generation of productive reservoirs is related to high-temperature upflows that are confined to faults or conduits, which also supply magma for magmatic extrusions and volcanoes (Fig. 1). This situation is typical of many high-temperature geothermal fields.

Multiyear, multidisciplinary studies of rhyolite tuffs at Yucca Mountain (12.5 Ma) [Pruess, 2001], which were conducted in connection with a feasibility study for storage of US nuclear waste, provided information on hydraulic and thermal properties of the tuffs and this may also prove useful for the present study.

Nevertheless, the mechanism that is responsible for the generation of permeable and porous volcanogenic reservoirs is not yet clear, as are the conditions that facilitate the transport and accumulation of oil-saturated fluids from the parent rock. The goal of the present study is to simulate the hydrothermal circulation for the Rogozhnikovskii and Mutnovskii reservoirs on a numerical model, including the estimation of fluid upflows at the existing temperature and pressure distributions in order to elucidate the mechanism for the generation of permeable reservoirs by hydrothermal circulation and reservoir self-sealing.

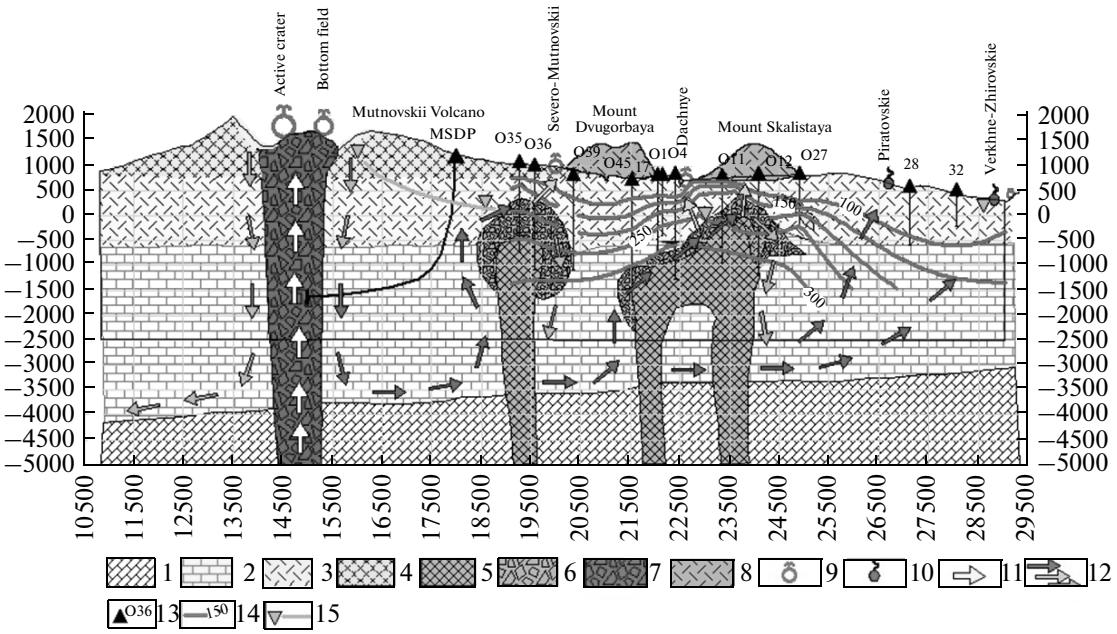

Fig. 1. A hydrogeologic section and conceptual model of the Mutnovskii Volcano–Mutnovskii geothermal field system: (1) crystalline basement, (2) Cretaceous basement and Miocene sandstone, (3) Neogene volcanogenic–sedimentary rocks, (4) Mutnovskii stratovolcano (Q_3–Q_4), (5) diorite intrusions, (6) contact zone of diorite intrusion, (7) magmatic plumbing system of Mutnovskii Volcano, (8) rhyolite and dacite extrusions (Q_3–Q_4), (9) fumarole fields, (10) hot springs, (11) magma and magmatic fluids, (12) hydrothermal fluids, (13) geothermal wells, (14) temperature distribution (Mutnovskii geothermal field), (15) ground water table in the Mutnovskii hydrothermal system (m, abs.) MSDP1 is a probable site where the first well to be drilled for the Mutnovskii scientific drilling project may be situated.

1. INPUT DATA FOR A NUMERICAL MODEL OF THE ROGOZHNIKOVSKII OIL-BEARING RESERVOIR

1.1. Geological Structure

The Rogozhnikovskii volcanogenic reservoir is situated in the Western Siberian Basin where volcanism dates back to 242–258 Ma [Korovina et al., 2010]. The area of rhyolites that formed during the Triassic Period in an environment of marginal continental volcanism or intraplate volcanism occupies 500 by 250 km^2 [Bochkarev et al., 2009]. Active fluid circulation is maintained in paleo-arc and paleo-rift systems in the Western Siberian Basin; the circulation leads to inversions of ground water mineralization and to hydrobaric temperature anomalies [Matusevich et al., 2005]. The oil field in the Rogozhnikovskii Triassic volcanogenic reservoir (rhyolite tuffs) lies at depths of 2.5–2.8 km, the reservoir is overlain by a sequence of poorly permeable clay–argillite deposits (Figs. 2, 3). The temperature in the reservoir is 120–140°C and the pressure is 290–310 bars. The isometric shapes of the positive hydrobaric and temperature anomalies suggest that the supply of fluids into the reservoir from below in zones that are marked by a funnel formation of the Triassic volcanogenic complex [Kiryukhin et al., 2008].

1.2. Percolation and Thermal Properties of the Reservoir

Laboratory investigations of the petrophysical properties of the Rogozhnikovskii volcanogenic reservoir gave 1.4 mD for permeability, 0.12–0.20 for porosity, and 2600–2800 kg/m^3 for mineral density. The relative permeability function for rock sampled from the volcanogenic reservoir is described in terms of the van Genuchten model for the aqueous phase ($m = 0.76$, $0.2 < S_{lr} < 0.5$) and by the Corey model for oil (for $0.3 < S_{or} < 0.4$), where S_{lr} is the residual saturation of the aqueous phase and S_{or} is that of the oil phase. The capillary pressure functions in rocks sampled from the volcanogenic reservoir are also described by the van Genuchten model (with the parameters $\lambda = 0.4438$, $S_{lr} = 0.22$, $1/P_0 =$ 1.50E-05 and Pmax = 50 bars). A detailed description of the parameters that the relative permeability function and capillary pressure involve can be found in [Pruess et al., 1999]. Laboratory tests of the core suggest that both hydrophilic and hydrophobic conditions may prevail; the latter may be due to large amounts of feldspar in the mineralogic composition.

According to FMI studies [Efimov et al., 2008], the reservoir is characterized by the following parameters of its fissure–block structure: the average block size is FS = 26 m, the average fissure separation is 0.17–0.5 mm (the mean is 0.3 mm), and the fraction of pore

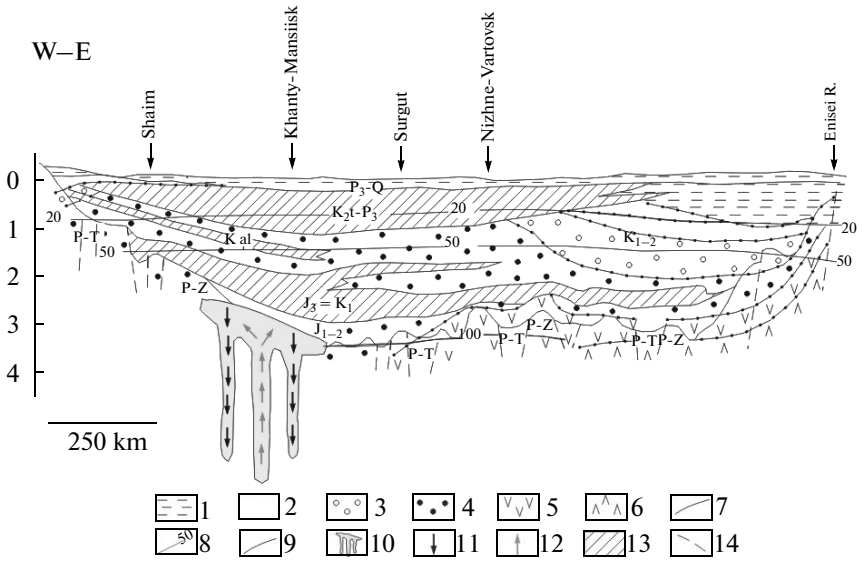

Fig. 2. Section of the Western Siberian megabasin with a schematic display of the Triassic volcanogenic reservoir and the conditions of circulation for fluids along the channels of buried volcanic structures [Kiryukhin, 2005] with some additions.
(1–6) hydrogeochemical zonality: mineralization <1 g/L (1), 1–3 g/L (2), 3–10 g/L (3), 10–35 g/L (4), 35–70 g/L (5), 70–150 g/L (6); (7) hydrogeochemical boundaries, (8) geoisotherms, °C, (9) lithologic interfaces, (10) volcanogenic reservoir, (11) separated, water downflows, (12) oil-saturated, ascending fluid flows, (13) aquifer rock sequences, (14) faults.

space in the volume is $FV = 3.17 \times 10^{-5}$. The permeability of the reservoir fissure space is estimated to be in the range 0.23–1.59 D (on the assumption that the fissures are plane-parallel and unfilled).

The reservoir's thermal conductivity is estimated from experiments that were carried out with cylindrical rock specimens with a diameter of 50 mm and a height of 50 mm; the data that were acquired from 29 laboratory experiments gave a mean thermal conductivity (under dry conditions) equal to 1.47 W/m °C and a mean specific heat capacity of 754 kJ/kg °C [Kiryukhin et al., 2012].

2. SIMULATING THE NATURAL STATE OF THE ROGOZHNIKOVSKII RESERVOIR

2.1. Simulating a Steady Thermohydrodynamical State

We sought to reproduce the observed distributions of temperature and pressure in the reservoir using iTOUGH2-EOS1 numerical modeling [Finsterle, 1999; Pruess et al., 1999].

At the first stage we made a 3D numerical model of the reservoir (10 × 8 × 3 km) on a 10 × 8 × 30 rectangular computational grid. The top layer in this model was assumed to have a fixed pressure of 10 bars and a fixed temperature of 5°C. In the lower layer we specified probable zones where a deep-seated heat carrier might penetrate, together with mass fluxes and enthalpies (sources) and probable downflow zones (sinks), as well as specified conductive heat sources at all elements in the lower layer. The iTOUGH2-EOS1 inversion modeling was used to estimate heat and mass fluxes and permeability (five parameters were to be estimated: conductive heat flux at the reservoir base, the permeability of the aquifer above the reservoir, the upflow discharge and enthalpy, and the downflow discharge). The model was calibrated at 41 points where the temperature was measured and at 20 points where the pressure was measured. The following best estimates of the parameters were obtained: 50.2 mW/m^2 for conductive heat flux, 0.0011 mD for the permeability of the overlying aquifer, 3.6 kg/s and 558 kJ/kg for the upflow discharge and enthalpy, and 3.6 kg/s for the downflow discharge. The modeled velocity field and the distributions of temperature and pressure show a positive anomaly of temperature and pressure associated with the upflow zone and a negative anomaly associated with the downflow zone.

The second stage of the simulation (see Figs. 3, 4) involved a finer computational grid (20 × 16 in plan view), with the base being divided vertically into 10 layers, the reservoir into 30 layers, and the overlying aquifer into 30 layers. The total number of elements in the model was 22400. The model was calibrated using 43 points of temperature measurement and 9 points of pressure measurement. The calibration points were tested using the iTOUGH2 built-in statistical methods. The model parameters to be estimated were (1) conductive heat flux at the base, (2) fluid upflow enthalpy, (3) discharge of the circulation in the reservoir (the upflow discharge was assumed to be equal to the downflow discharge), and (4) the reservoir permeability. Inversion simulation (option #7B6) gave the following best esti-

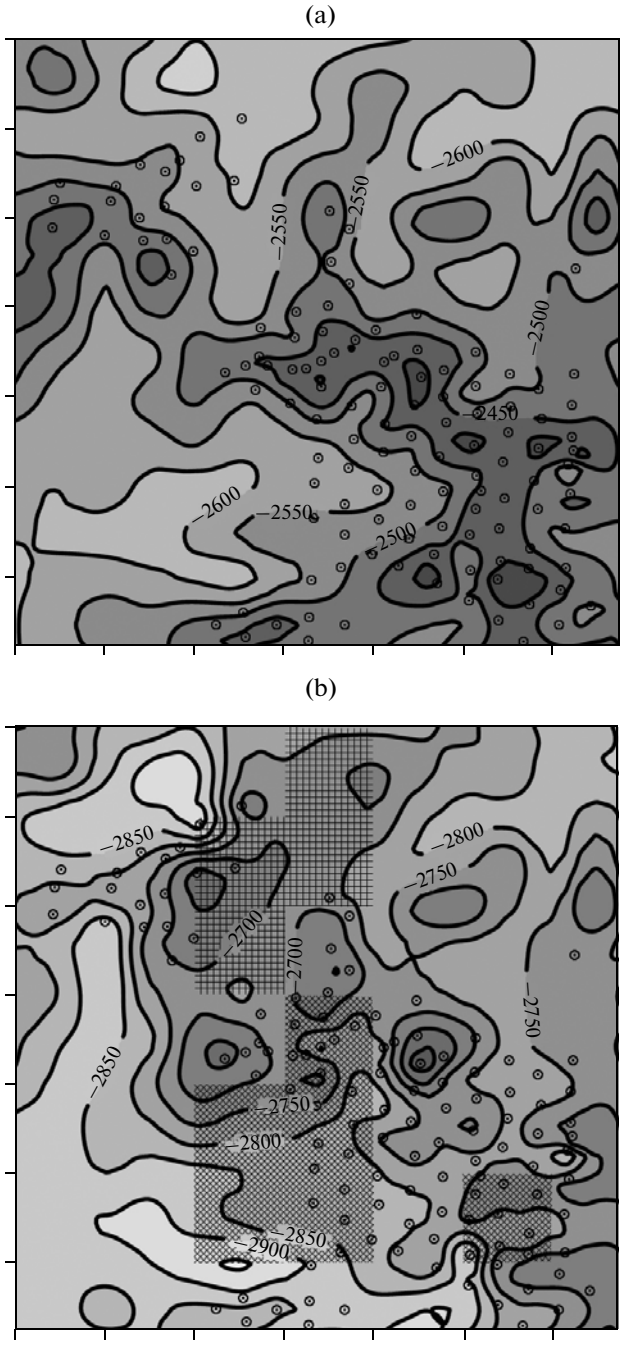

Fig. 3. A fragment of top surface (m, abs.) of the Rogozhnikovskii rhyolite reservoir (top) and of the bottom (below). The diagonal shading in the reservoir bottom shows supposed zones where deep-seated heat carrier comes from below, crossed shading denoting zones of water downflow. The sites where wells reach the rhyolite reservoir are shown by circles. All are at intervals of 1 km.

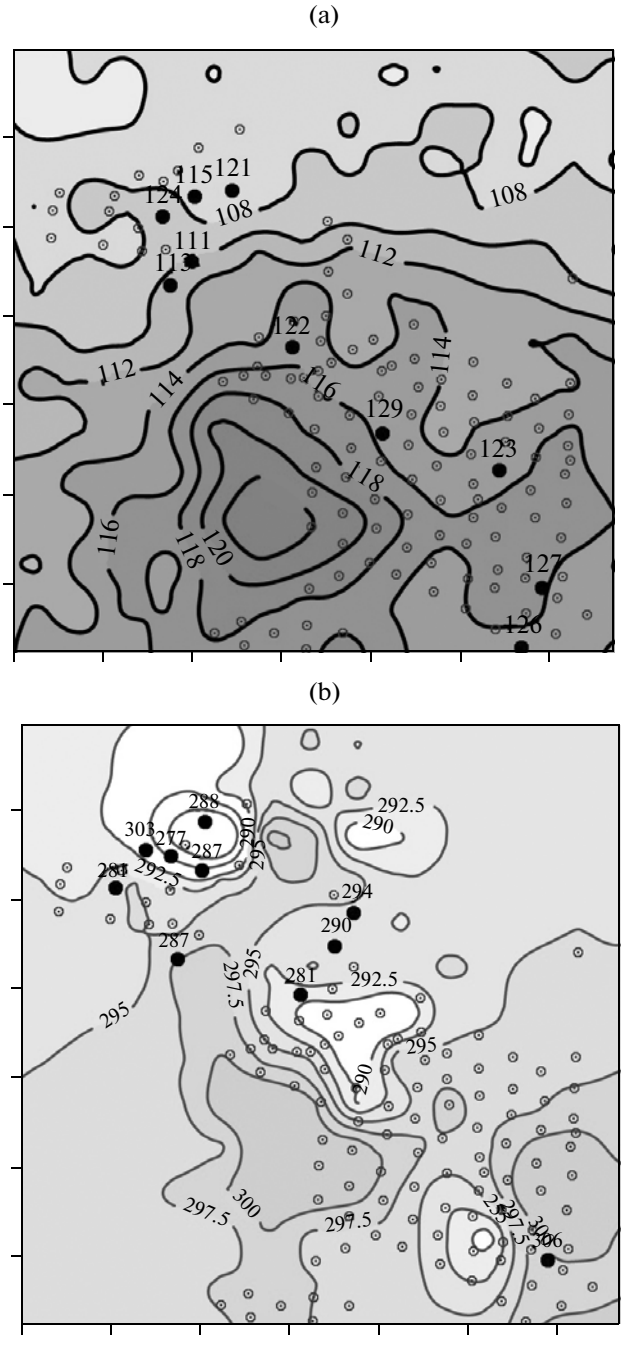

Fig. 4. Results of iT2-EOS1 inversion simulation.
(a) temperature distribution (°C) in the middle of the rhyolite reservoir (the 25th layer of the model, the average abs. height is 2650 m), also shown are temperatures in the wells (the interval measured is −2700 to −2500 m abs.), and the models used for calibration; (b) pressure distribution (in bars, converted to −2600 m abs.) in the middle of the rhyolite reservoir, also shown are horizontal components of mass heat-carrier flow vectors and converted pressure values used for model calibration. The sites where wells reach the rhyolite reservoir are shown by circles. All are at intervals of 1 km.

mates: 40.0 mW/m^2 for conductive heat flux, 2.6 mD for reservoir permeability, 3.6 kg/s for circulation discharge, and 607 kJ/kg for upflow enthalpy. The resulting rms uncertainties for temperature (4.8°C) and pressure (3.6 bars) are in overall agreement with the assumed measurement errors for these quantities. The most sensitive model parameters were conductive heat flux and upflow enthalpy; we found a significant correlation between enthalpy and circulation discharge

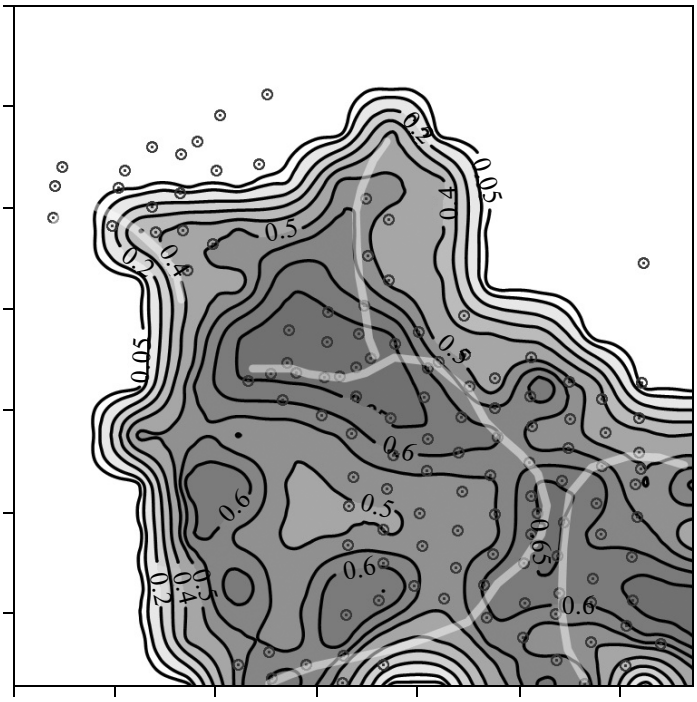

Fig. 5. Results of iT2-EOS10 inversion simulation: the distribution of oil phase saturation at the top of the rhyolite reservoir (the 40th layer of the model). Heavy lines show the axes of "volcanic ridges" that correspond to watersheds at the top of the rhyolite reservoir (see Fig. 3). The sites where wells have reached the rhyolite reservoir are shown by circles. All are at intervals of 1 km.

(0.97), which limits our possibilities for accurate simultaneous estimation of these parameters.

2.2. Simulating the Oil Saturation of the Reservoir

We sought to reproduce the observed oil saturation in the reservoir by using the iTOUGH2-EOS10 (T2VOC) simulation tools [Falta et al., 1995; Finsterle, 1999]. The initial distributions of temperature and pressure were based on the conditions that were derived from thermohydrodynamic simulation, with the initial saturation of the oil phase being assumed to be zero. Dirichlet boundary conditions of the first kind were specified at the top of the reservoir. The boundary conditions for fluid upflow into the reservoir in the lower layer were modified; the aqueous phase with a discharge of 3.6 kg/s was replaced with an oil phase with the same discharge. The problem was solved in the isothermal regime with a reference density of the oil phase equal to 730 kg/m^3. The initial simulation scenario assumed the van Genuchten functions for the aqueous phase as the relative permeability functions (S_{lr} = 0.23) and the Corey functions for the oil phase (S_{or} = 0.4), with the capillary pressure function being zero.

The simulation revealed that saturation with the oil phase of the reservoir fragment under consideration occurs during 50000 years; by that time the oil resources reach about 300 million tons and no significant addition to the oil mass available in the reservoir occurs later, due to the oil that seeps through the top. The oil phase mostly propagates along the fluid lines of flow, with the oil filling both positive and negative structures that are not isolated by the watersheds of volcanic ranges (Fig. 5). Comparison between simulated and actual saturations of the oil phase based on 42 calibration points (the calculation was carried out by GIS interpretation) shows an average consistency (–0.03).

3. THE HYDROGEOCHEMICAL MECHANISM FOR THE GENERATION OF PRODUCTIVE RESERVOIRS IN VOLCANOGENIC ROCKS

3.1. A 3D TOUGHREACT Model of the Rogozhnikovskii Oil Reservoir

3.1.1. Assembling the Model and Simulation Results

Hydrothermal circulation considerably affects the chemical and mineral compositions, pore space structure, permeability, and capacity of a reservoir. There are cases in which the filtration and capacity properties are improved (e.g., when volcanogenic rocks are transformed into secondary quartzite, the permeability and porosity increase), while in other cases deterioration results (e.g., permeability decreases when volcanogenic rocks are transformed into clay and aquifers are generated) [Korzhinskii, 1982]. The principal factors that control rock changes under hydrothermal processes include the initial state of volcanogenic rocks (mineral composition, porosity, and permeability), temperature,

pressure, the phase and chemical composition of the circulating fluids, and the time that the fluid–rock chemical interaction lasts. The 3D structure of permeability in a reservoir under consideration also substantially affects the rate and degree of hydrothermal alteration.

The Rogozhnikovskii reservoir is composed of high-silica volcanogenic rocks that are strongly fractured and involve faults that are not infrequently transformed into breccia. The petrophysical properties of the Rogozhnikovskii reservoir were described in detail in [Shadrina et al., 2008; Shadrina, 2009]. The hydrothermal alteration in question includes the early alkaline phase of K-feldspar albitization, which generates albite and biotite, and the acidic phase, which involves the dissolution of quartz and K-feldspar and generates secondary cavities. Pelitization, fluoridization, carbonatization, chloritization, and silicification of cracks and pores occurred during the earlier phases of the processes with some temporal lags. The processes of the late alkaline phase are poorly expressed; they involve the generation of K-feldspar and hematite micrograins in the lower section in both the matrix and the cracks. All the hydrothermal processes referred to above are superimposed on one another and occur to varying degrees in different parts of the Rogozhnikovskii reservoir, giving rise to a mosaic structure of metamorphic processes.

A 3D rectangular model was used for the Rogozhnikovskii volcanogenic reservoir in order to elucidate the mechanism that was responsible for the generation of permeability and porosity. This is a $500 \times 500 \times 400$ m^3 model and includes 100 elements (Fig. 6). The three lower layers in the model (with a total thickness of 300 m) make a reservoir of rhyolite tuff (initial porosity of 0.17, initial permeability of 1 mD, and mineral density of 2600 kg/m^3), the upper layer is an aquifer at a constant temperature of 100°C and a pressure of 200 bars. The initial distributions of temperature and pressure in the reservoir are consistent with a conductive heat flux of 60 mW/m^2 and hydrostatic conditions. The upflow of the high-temperature heat carrier was specified in an element of the model (#11) with a mass discharge of 1 kg/s and enthalpy 1090 kJ/kg; discharge from the reservoir in the form of a downflow was also specified to be at a rate of 1 kg/s, but in a different element of the model (#15). Model element #37 was used to monitor the evolution of parameters in a transient-state reservoir. Hydrothermal circulation in the reservoir was maintained in the model during a long period of simulation (1.8 Ma).

Chemical interaction between the heat carrier and host rocks was simulated using the TOUGHREACT code [Kiryukhin et al., 2004; Xu et al., 2006], which supplements the TOUGH2 code [Pruess et al., 1999]. The TOUGHREACT code incorporates diffusion and convective transport of dissolved chemical components; a local chemical equilibrium is assumed in the liquid phase. The dissolution of original minerals and the generation of new minerals were calculated incorporating the kinetics of mineral generation using the following discharge law:

$$r = kS(1 - Q/K)\exp(Ea/(R \cdot 298.15) - Ea/(RT)),$$

where k is the kinetic constant of chemical dissolution/precipitation at 25°C, mol/s · m^2, S is the specific surface of chemical interaction, m^2/m^3; Q is the product of activities; K is a constant of equilibrium for the water–rock system considered here; E_a is activation energy. kJ/kmol; R is the universal gas constant, kJ/kmol K; and T is the temperature, K. Our calculations of chemical reactions incorporated the fact that the respective constants are functions of temperature. In the present study all kinetic parameters of fluid–rock interaction were specified as in Problem 8.7 *Hydrothermal Alteration of Upper Aquifer. Caprock Alteration* [Xu et al., 2006].

The variation of the permeability "k" in relation to porosity φ is described by the simplified Carman–Kozeny relation:

$$k = k_i \cdot (1 - \varphi_i)^2 \cdot \varphi^3/(1 - \varphi)^2/\varphi_i,$$

where k_i is initial permeability, 0.9 mD, φ_i is initial porosity, 0.17. The Carman–Kozeny relation postulates an exponential increase of permeability with increasing porosity.

The initial mineral composition of the volcanogenic reservoir was specified as volcanic glass (glass3) (the TOUGHREACT thermodynamic database), while the secondary minerals include quartz, K-feldspar, high albite, low albite, alpha cristobalite, chlorite, illite, laumontite, mordenite, Ca-smectite, Mg-smectite, and Na-smectite. The chemical composition of the aqueous phase in the original fluid and in the fluid that is supplied to the reservoir was specified as follows: pH = 7.7, Na^+ 7380 mg/kg, K^+ 280 mg/kg, Ca^{2+} 52 mg/kg, Cl^- 10 871 mg/kg, SO_4^{2-} 7 mg/kg, HCO_3^- 2192 mg/kg, and SiO_2 105 mg/kg (corresponding to the average composition of the aqueous phase in deep wells).

Below, we describe the results for the simulation option #6E-3B. Figures 7, 8, and 9 show the evolution of thermohydrodynamic and filtration–capacity properties, as well as the mineral composition of the simulated reservoir for the time interval 0–1.8 Ma from the start of reservoir generation until the end, which is associated with self-sealing by secondary hydrothermal minerals.

Pressure and temperature. The permeable reservoir is characterized by a temperature that increases to 210–250°C and a pressure as high as 226 bars during most of the simulation time (0–1.8 Ma), except for the short

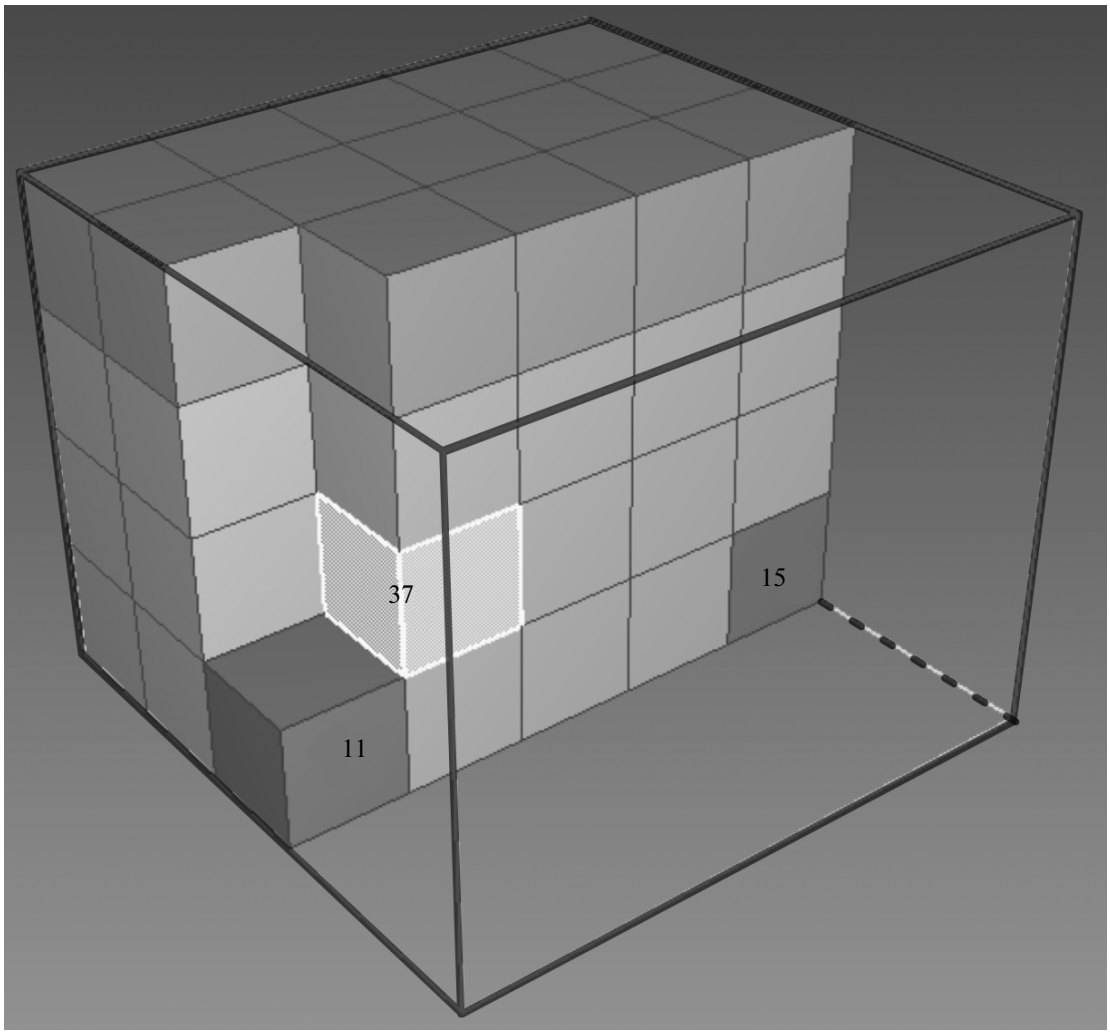

Fig. 6. A fragment of the 3D model for analysis of geochemical evolution of the Rogozhnikovskii reservoir: (11) an element of the model from the region of deep heat-carrier upflow, (15) an element of the model from the downflow region (discharge), (37) an element of the model from the producing reservoir.

period during the first phase of circulation when boiling occurs.

Porosity and permeability substantially increase: from 0.17 to 0.34–0.45 and from 1 mD to 50 mD, respectively, as a result of water–rock interaction during hydrothermal circulation, which is characterized by dissolution of the original volcanic glass and the generation of secondary minerals (quartz, K-feldspar, and albite). Figure 7 shows the evolution of porosity at three characteristic points of the hydrothermal system (the upflow zone, the discharge zone in the form of a downflow, and the productive reservoir) in semilogarithmic time-dependent plots and Fig. 8 shows the distribution of porosity in a vertical section of the model by the end of the simulation.

The evolution of secondary hydrothermal minerals. Quartz forms on the outer boundaries of the permeable reservoir in the downflow zone, where the mineral fraction reaches a value of 0.45 by the end of the simulation time. K-feldspar traces the head part of the permeable reservoir where its mineral fraction reaches 0.189 by the end of the simulation time. The presence of albite was noted in the zone of downflow from the reservoir, with that zone being adjacent to the part of the reservoir with the highest permeability and porosity, with the mineral fraction reaching 0.256. Chlorite is distributed throughout the entire zone of hydrothermal circulation, where its mineral fraction reaches 0.0016. The mineral fraction of illite may reach a few percent during the first phase of hydrothermal circulation; after a lapse of 0.18 Ma this mineral can only be observed in the low-temperature zone of the downflow, where its mineral fraction is below 0.002; later, the mineral disappears completely. Zeolites (laumontite, wairakite, and mordenite) form in the low-temperature zone of the downflow during the first phase of hydrothermal alter-

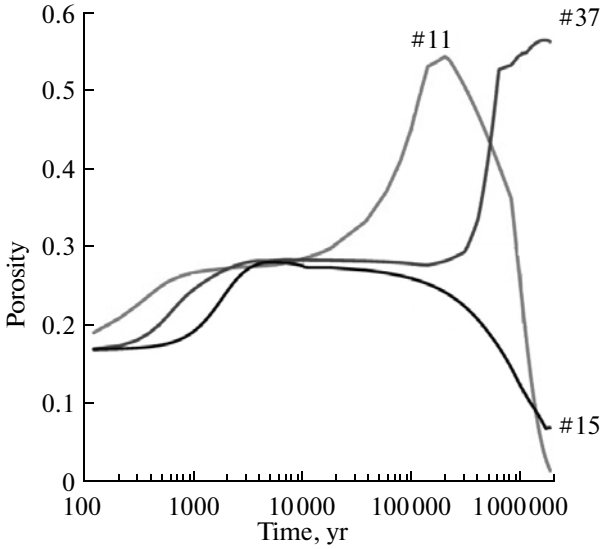

Fig. 7. Porosity variation during the evolution of the hydrothermal system based on THC simulation: (11) region of deep heat-carrier upflow, (15) downflow region (discharge), (37) producing reservoir.

ation (0–0.2 Ma) but disappear from the reservoir by the end of the simulation time. Calcite is generated during the last phase of hydrothermal circulation (1.8 Ma), by that time its mineral fraction reaches 0.642 in the high-temperature upflow zone (model element #11), which results in a final self-sealing of the permeable rhyolite reservoir (see Fig. 8). Figure 9 shows changes in mineral content in an element of the permeable reservoir model (#37) during the evolution of the hydrothermal system.

One notes that a short-lived drop in pressure (down to 20–30 bars) and boiling are observed in the model during the earlier phase of hydrothermal circulation (in the interval from 600 to 6000 years). This can be explained by a rapid and considerable increase in porosity (from 0.17 to 0.28) due to the transformation of volcanic glass to quartz and albite. This short-lived period of "vacuum" may favor the inflow of the oil phase into the permeable porous reservoir from the host rock and its long-term storage in the rhyolite reservoir.

3.1.2. Comparison between the Results of Thermohydrodynamic–Chemical Simulation of the Evolution of the Rogozhnikovskii Reservoir and the Observations

The actually observed hydrothermal alteration in the Rogozhnikovskii rhyolite reservoir is characterized by a really non-uniform distribution of secondary minerals (albite, K-feldspar, and quartz) over the section. One notes regions of dominant albitization, replacement of rocks with K-feldspar, and silicification. According to observations on microsections, albitization involves much larger areas compared with the two other processes (these observations are based on descriptions of thousands of microsections). Elemental photographing

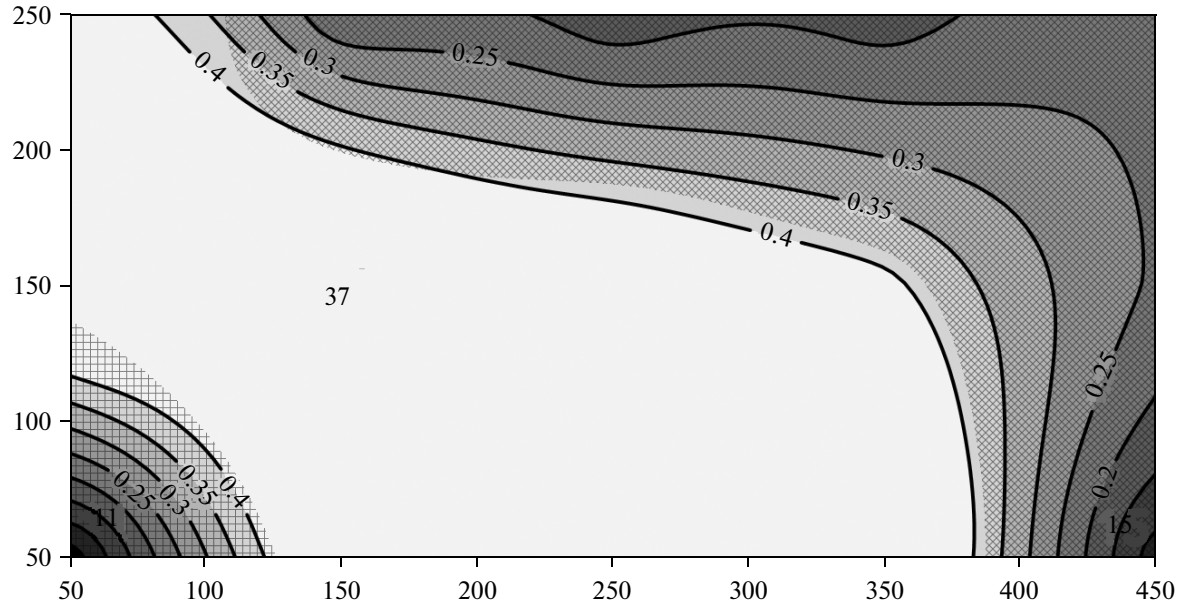

Fig. 8. Distributions in the simulated reservoir after the lapse of 1.8 Ma since the start of hydrothermal circulation: porosity (shown by isolines, with the initial porosity being 0.17), the volume fraction of secondary quartz is above 0.2 (shown by diagonal shading), the volume fraction of calcite is above 0.5 (shown by cross hatching), (11) an element of the model from the region of deep heat-carrier upflow, (15) an element of the model from the downflow region (discharge), (37) an element of the model from the producing reservoir. All are at intervals of 1 m; the distributions are shown in the Y = 250 m vertical section.

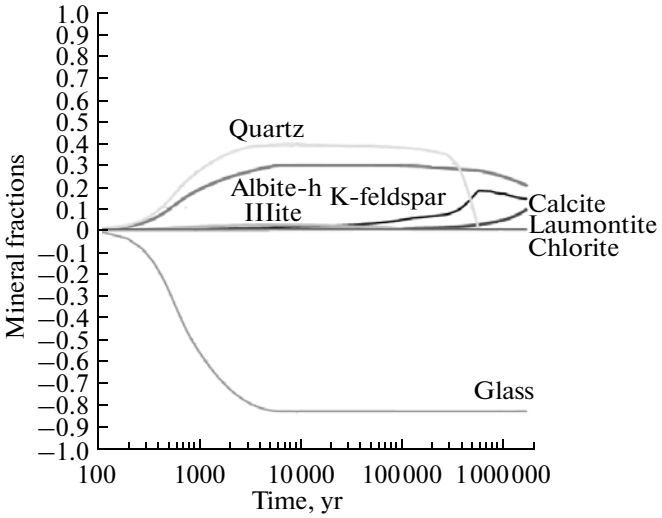

Fig. 9. Variation in the fraction of mineral phases during the evolution of the hydrothermal system based on results of THC simulation in a producing reservoir (model element 37).

of effusive rock specimens with different structural and textural characteristics in an electron microscope shows (as does a color map that displays the distribution of chemical elements) that albitization involves the entire rock volume irrespective of its structural features. Silicification occurs in large perlite forms and cracks, also partly in fluids. Late K-feldspar is deposited on small perlite forms in rocks of massive structure and on fluids without involving perlite jointing in rocks of a fluidal structure (that is, fluidal porosity has greater openness compared with perlite porosity). Chlorites are found everywhere throughout the entire volume of the volcanogenic rock sequence, while zeolites were not present at all. Well-expressed hydromica (illite) is present and occasionally in considerable amounts (as much as 5 vol %) in the rock as the final product of feldspar pelitization. Illite is naturally found in the greatest amounts in regions of the greatest permeability. Another reason that illite might be generated lies in smectite dehydration [Kireeva, 2010]. Nevertheless, our simulation shows a limited period of illite generation. Calcite and breinerite are precipitated in fissures during the last phase of hydrothermal circulation, thus sealing the permeable reservoir.

Analyses of the effects of secondary hydrothermal processes (hydromicatization, chlorization, pelitization, and albitization) on the variation of porosity, permeability, bulk density, and wettability are combined in the table. The generation of illite and chlorite does not affect the reservoir properties. Pelitization and the generation of K-feldspar reduce the filtration and capacity properties of the reservoir. In contrast to the above, albitization enhances permeability and porosity, which is consistent with the simulation results. The wettability of mineral grains depends on the type of hydrothermal alteration. High-temperature albitization leads to the generation of a hydrophobic reservoir, while low-temperature hydrothermal processes enhance its hydrophilic properties. It thus appears that hydrothermal processes, which are non-uniform in the reservoir volume, significantly affect the filtration and capacity properties of the Rogozhnikovskii volcanogenic reservoir.

3.2. A 3D MODEL OF THE MUTNOVSKII GEOTHERMAL RESERVOIR, KAMCHATKA

Assembling the Model and Simulation Results

The Mutnovskii geothermal field was used for thermohydrodynamic TOUGHREACT simulation in order to reach a better understanding of the conditions that favor the generation of a permeable and porous reservoir, because the Mutnovskii reservoir has been extensively drilled, subjected to production testing and long-term maintenance (2000–2010), and is considered to be a well-known reservoir [Kiryukhin, 1996]. The host rocks around the reservoir are diorites, Miocene/Pliocene sandstone, rhyolite and andesitic tuffs and lavas. The deep-seated heat carrier is a one-phase flow (54 kg/s, above 280°C, 1390 kJ/kg) that rises from the southeastern sector of the field. The initial thermohydrodynamic

Correlation coefficients in the processes of secondary alteration and the permeability–storage–porosity (PSP) of rocks and the wettability of the grain surface

Secondary processes	Hydromicatization (36)	Chlorization, pelitization (32)	Pelitization, chlorization, hydromicatization (57)	Pelitization, microclinization, albitization (98)	Albitization, pelitization, chlorization, leaching (102)
Porosity	–0.31	–0.13	–0.62	–0.56	0.84
Permeability	–0.1	–0.09	–0.26	–0.86	0.33
Bulk density	0.16	0.32	0.61	0.56	–0.83
Wettability	–	–	0.11–0.51 (9)	–	0.54–0.9 (8)

Note: Hydromicatization (the controlling process) involves 30–80 vol % of the rock; the values are 10–30 vol % for chlorization and pelitization and below 10 vol % for the combined pelitization, chlorization, microclinization, and albitization; sample size is enclosed in parentheses. The wettability of grain surface: >0.5 on hydrophobic and <0.5 on hydrophilic surfaces.

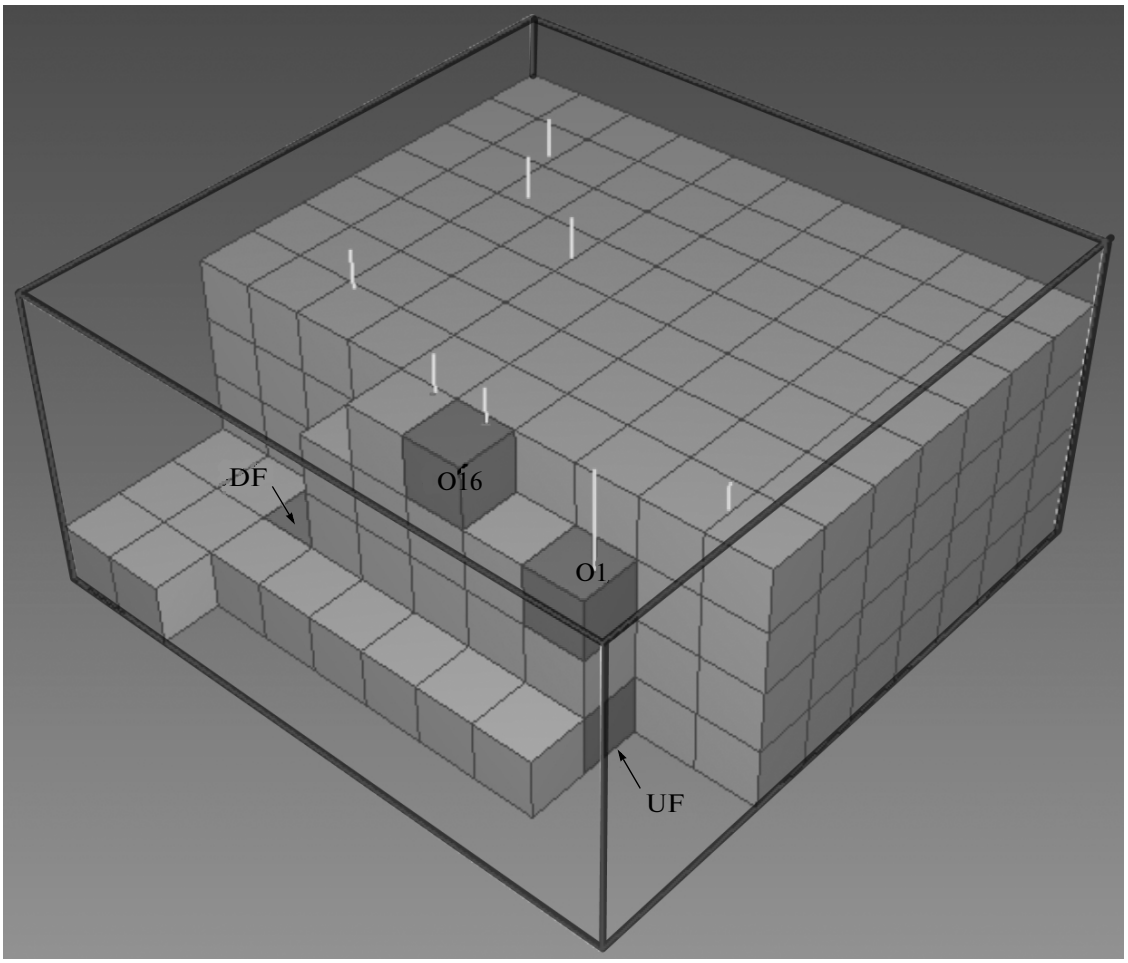

Fig. 10. Geometry of the 3D model for the Dachnyi area in the Mutnovskii geothermal field. The highlighted elements of the model denote the zone of heat-carrier upflow (UF, Upflow), the producing water-dominated reservoir (O1), the producing steam-dominated reservoir (O16), and the zone of separated water downflow (DF, Downflow).

conditions for a TOUGHREACT model were specified based on a previously developed 3D rectangular model consisting of 503 elements [Kiryukhin, 1996] (Fig. 10).

The chemical composition of the aqueous phase in the original fluid and in the deep-seated fluid that comes into the reservoir is as follows: pH = 7.4, Na^+ 168 mg/kg, K^+ 32 mg/kg, Ca^{2+} 1.4 mg/kg, Cl^- 198 mg/kg, SO_4^{2-} 85 mg/kg, HCO_3^- 57 mg/kg, and SiO_2 723 mg/kg (the average chemical composition was based on samples from well 029W). Much of the rocks that compose the Mutnovskii reservoir (40%) consists of rhyolite tuffs, hence the original mineral composition that was specified for the model as "volcanic glass" (glass3) (100%). The possible secondary minerals include quartz, K-feldspar, high albite, low albite, sanidine-α, alpha cristobalite, calcite, chlorite, cristobalite, illite, laumontite, mordenite, wairakite, kaolinite, Ca-smectite, Mg-smectite, and Na-smectite.

The evolution of filtration and capacity properties and mineralogical composition as they change under hydrothermal alteration was considered for the time interval from 0 to 1 Ma and later. The simulation results were continuously recorded to monitor the characteristic elements of the model that correspond to the upflow zone of the deep-seated heat carrier (UF), productive water-dominated reservoir (O1), productive steam-dominated reservoir (O16), and the downflow zone of separated water (DF) (see Fig. 10), as well as for discrete times (1000, 10000, 20000, 50000, 100000, and 500000 years and so on as far as the simulated infinity) throughout the model volume.

The overall picture of the evolution of the productive reservoir emerges as follows.

Temperature, pressure and steam saturation: the maximum temperature decreases from the initial value of 309°C to 300°C (10 ka), 288°C (20 ka), 281°C (1 Ma), then slowly increases to reach 303°C (at infinite time), while the maximum pressure decreases from

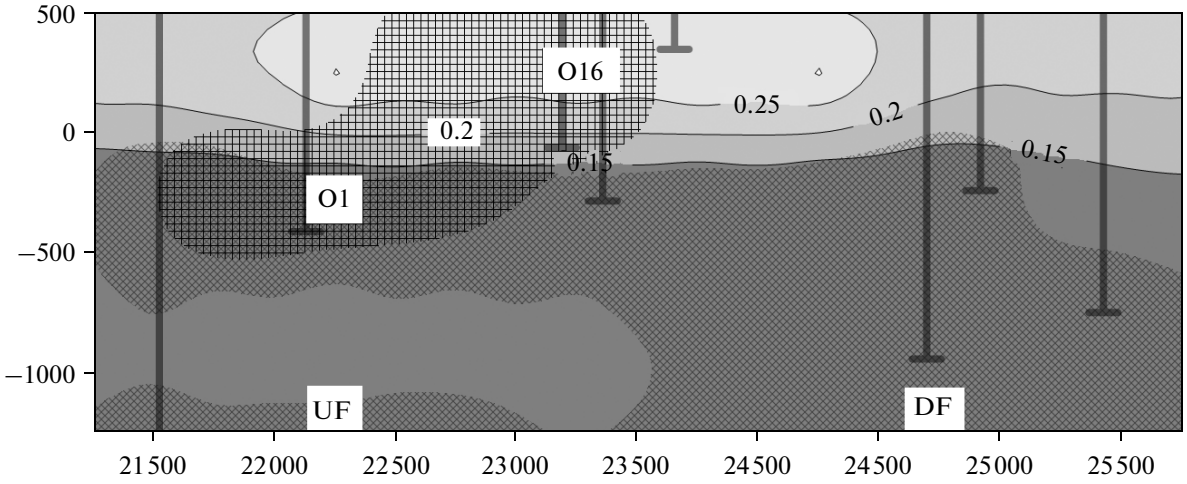

Fig. 11. Porosity distribution in the Mutnovskii reservoir based on results of THC simulation (time ∞) in the vertical X = 45 250 m cross-section (see Fig. 10). Diagonal hatching marks the zone of secondary quartz with a volume fraction of more than 0.44, the cross hatching shows the region of two-phase heat carrier (steam saturation above 0.03). The initial porosity distribution was as follows: 0.02 in the interval between −1500 and −1000 m, 0.03 between −1000 and −500 m, 0.08 between −500 and 0 m, and 0.2 between 0 and 500 m abs. The highlighted model elements represent the zone of deep heat-carrier upflow (UF, Upflow), the producing water-dominated reservoir (O1), the producing steam-dominated reservoir (O16), and the zone of separated water downflow (DF, Downflow) (see Fig. 10).

141 bars to 125 bars (1000 yr), 115 bars (10 ka), 112 bars (10 Ma), then slowly increases to reach 139 bars (at infinite time), the maximum steam saturation increases from 0.245 to 0.322 (10 ka), 0.331 (50 ka), 0.341 (500 ka), then decreases to 0.079 (at a model time of ∞).

The porosity constantly increases from 0.20 (the initial value) to 0.29 in the two-phase zone; this zone gives rise to porous reservoirs (0.2–0.25) (Fig. 11). In zones of water-dominated hydrothermal circulation the porosity increases by factors of 2–5 (50 ka) and then stabilizes (Fig. 12).

The most significant increase in permeability occurs in the high-temperature upflow zone and in the downflow zone, from 0.3 mD to 40–50 mD (50 ka); afterwards the permeability slowly decreases to terminate in a final sharp drop in the downflow zone. The productive reservoir shows a similar tendency of permeability variation: an initial rise from 1.5 mD to 12 mD (in a water-dominated reservoir) and from 5 mD to 23 mD (in a steam-dominated reservoir); afterwards, the permeability decreases.

The results from simulating hydrothermal alteration in the Mutnovskii reservoir can be described as follows (Fig. 13). The initial volcanic glass (glass3) is rapidly transformed into various mineral phases; the most intensive transformation occurs in the high-temperature upflow zone where its volume fraction decreases from 98% to 82% (1 ka), 20% (10 ka), 4% (20 ka), and 0% (at model time of ∞). At the same time, the initial fraction of glass in zones of low permeability (0.001 mD) and slow circulation remains constant. Albite forms synchronously with quartz, at first in the upflow zone: 5% (1000 years), 26% (10 ka), 30% (20 ka), 32.4% (200 ka), and afterwards (500 ka) uniformly spreads throughout the lower part of the reservoir (below 0 m abs.) as far as the downflow zone. The maximum volume fraction of albite is 32.4%. Quartz intensively forms during the first phase in the upflow zone: 7% (1000 years), 35% (10 ka), 41% (20 ka), 43.5% (200 ka), then (500 ka) uniformly spreads throughout the entire lower part of the reservoir (below 0 m abs.) as far as the downflow zone. The maximum volume fraction of quartz is 43.5%. Cristobalite was detected in the model in insignificant amounts (below 0.0016%) in the marginal parts of the reservoir during the earlier phases of reservoir generation (1000 years). No amorphous silica was detected in the model. K-feldspar behaves similarly to quartz and albite, but shows substantial deceleration in the upflow zone and in the productive part of the reservoir. At first, K-feldspar was deposited in the upflow zone: 0.2% (1000 years), 1.2% (10 ka), 1.5% (20 ka), 1.7% (200 ka), 2.1% (2 Ma); afterwards it began to spread throughout the entire lower part of the reservoir (below 0 m abs.) as far as the downflow zone and again concentrated in the upflow zone (4.8%, at infinite time). Chlorite was detected in the lower part of the reservoir during a limited time only (about 10 ka) at low volume concentrations below $6 \cdot 10^{-6}$%. Illite spread in the tracer "discrete start-up" from the upflow zone to the downflow zone, "penetrated," and was distributed in poorly permeable peripheral zones. Its maximum volume concentrations in the reservoir were 0.1% (1000 years), 0.8% (10 ka), 1.2% (20 ka), and 1.7% (50 ka). In the final

account illite accumulated in the O16 steam-dominated productive reservoir and in poorly permeable zones (below 2.2%), with its volume concentration decreasing to zero in the O1 zone of water circulation. Zeolites formed embedded zones. Wairakite was generated in the inner part, which was identical with the upflow zone and the zone of the water-dominated reservoir, with the concentration of wairakite reaching its maximum at 0.98% (200 ka); it then decreased to 0.7% (at infinite time). Laumontite occupied poorly permeable zones with slower fluid circulation, as well as fixing the bottom of two-phase reservoirs, with its maximum concentration reaching 1.1% (at infinite time). Mordenite behaved like laumontite, with its volume concentration reaching 2.8% (at infinite time). Na-, Ca-, and Mg-smectites formed in the upflow zone where their volume concentrations gradually increased to reach 1.1%, 0.6%, and 0.4%, respectively (1 Ma). Afterwards, the smectites spread from the upflow zone to the adjacent parts of the reservoir (Ca-smectite) or moved to those parts completely (Na-smectite), or else disappeared completely (Mg-smectite). Kaolinite spread during 50 ka from the upflow zone throughout the entire reservoir below 0 m abs., reached its maximum volume concentration (12.5%) and remained in that state to the end (to infinite time). Calcite accumulated (below 0.00056%) in poorly permeable peripheral parts in the lower reservoir (at infinite time). Figure 13 illustrates the above discussion and shows the evolution of the mineral composition in the water-dominated productive reservoir.

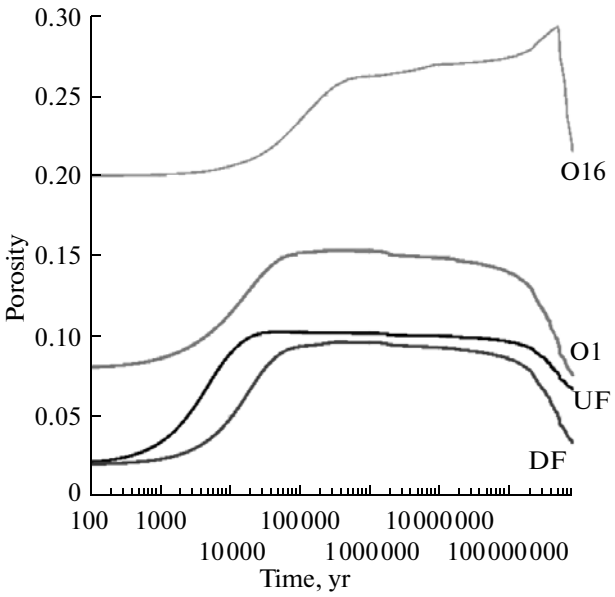

Fig. 12. Porosity variation during the evolution of the Mutnovskii geothermal reservoir based on results of THC simulation: UF is the region of deep heat-carrier upflow, DF is the downflow region (discharge region), O1 is the producing water-dominated reservoir, and O16 is the producing steam-dominated reservoir.

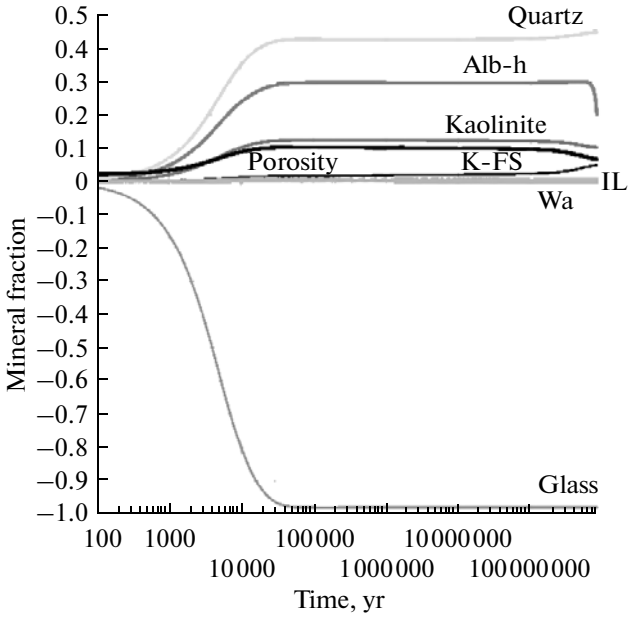

Fig. 13. Variation in the relative amounts of mineral phases and porosity during the evolution of the Mutnovskii geothermal reservoir based on results of THC simulation in the region of deep heat-carrier upflow (UF).

3.2.2. Comparison between the Results of Thermohydrodynamic and Chemical Simulation of the Evolution of the Mutnovskii Reservoir and the Actual Data

Analysis of the actual data that relates to the distribution of secondary hydrothermal minerals in the productive reservoir of the Mutnovskii geothermal field shows that the deeper one-phase reservoir is characterized by an association of quartz, chlorite, epidote, and pyrite; the steam-dominated two-phase reservoir (above 0 m abs.) is characterized by an association of wairakite and quartz; the outer steam–condensate zone includes an association of illite, chlorite, and calcite [Slovtsov, 2001].

Mineralogical and petrographic studies of the material that was extracted from three drilled additional wells (2002–2003) suggest the following: the original rocks are subjected to intensive hydrothermal alteration. The secondary hydrothermal minerals in the productive zone are dominated by chlorite and wairakite, as well as by iron and titanium oxides. Epidote, prehnite, adularia, and albite are present in insignificant concentrations. Wairakite (together with quartz) fills in the rock cavities, as well as replacing plagioclase phenocrysts. Chlorite is generated due to the alteration of the groundmass in intimate association with the quartz–feldspar mass and oxides. Hydrothermal alteration in

the Mutnovskii reservoir is estimated as the result of a multiphase process.

Although the analogy between a natural and a modeled object is incomplete, some of the parameters show satisfactory agreement, including the generation of quartz, albite, K-feldspar, and wairakite in the upflow zone and in the adjacent productive reservoir, and the filling of poorly permeable rock masses that surround the productive reservoir with illite.

CONCLUSIONS

(1) The volcanogenic oil basin is situated in western Siberia, lies in Permian/Triassic rocks (rhyolite tuffs) at depths of 2.5–2.8 km, and has a temperature of 120–140°C and a pressure of 290–310 bars. We used thermohydrodynamic inversion simulation for the diagnostics of deep hydrothermal circulation in the Rogozhnikovskii volcanogenic oil reservoir in western Siberia to show that the distribution of the temperature and pressure observed at depths of 2.5–2.8 km in the reservoir can be explained by hydrothermal circulation with a discharge of 3.6 kg/s and an enthalpy of 607 kJ/kg (144°C). The upflow zones are associated with positive anomalies of temperature and pressure, while the downflow zones are associated with negative anomalies. The circulation zones indicated above may coincide with the paleovolcanic plumbing systems of conduits or with other permeable features in the basement.

(2) Simulation of natural filling for the Rogozhnikovskii reservoir with oil as it came to the reservoir in the form of an upgoing fluid flow showed that the oil phase propagates along lines of flow and fills both uplifted volcanic ridges and buried relief forms (calderas) on the top of the volcanogenic reservoir.

(3) The mechanism for the generation of productive reservoirs in rhyolites can be explained in terms of TOUGHREACT simulation by long-term hydrothermal circulation involving chemical water–rock interaction, which enhances the permeability–porosity along high-temperature flows and terminates in a final self-sealing of the resulting productive reservoir. The parameters that are observed at present, which include pressure, temperature, phase conditions, the distribution of permeability–porosity, the chemical composition of fluids, and the hypothetical mineral composition of the initial rock (volcanic glass), are all used as input data for subsequent TOUGHREACT simulation. The simulation of the Rogozhnikovskii reservoir shows that long-term hydrothermal circulation leads to higher porosity (2.64) and permeability(×50) because the original volcanic glass was replaced by quartz, albite, and K-feldspar; the earlier phase of hydrothermal circulation (<10 ka) involves boiling and a considerable drop in pressure, while the terminal phase is characterized by considerable deposition of calcite at the base of the upflow, which leads to self-sealing of the reservoir. Simulation for the Mutnovskii reservoir shows that 50 ka of hydrothermal circulation leads to greater porosity (×5) and greater permeability (×13) accompanied by an increased two-phase (steam + water) zone and a pressure drop (down to 16 bars); the generation of a productive reservoir is marked by quartz, K-feldspar, albite, and wairakite. Both of these scenarios demonstrate the possible generation of productive reservoirs due to alteration of the original mineral composition in rhyolite caused by hydrothermal circulation and exhibit conditions of a short-lived pressure drop during the earlier phase of reservoir generation (which favors the attraction of oil and ore-forming fluids into the reservoir). Reservoir self sealing during the last phase of hydrothermal circulation favors the accumulation and detention of fluids in the productive reservoir and the formation of mineral deposits.

ACKNOWLEDGMENTS

We thank T.A. Korovina, A.Yu. Baturin, E.V. Nikolaeva, A. Battistelli, S. Finsterle, V.G. Rumynina, S.L. Shvartseva, and B.N. Ryzhenko for helpful comments and suggestions. This work was supported by the Russian Foundation for Basic Research, project no. 129-05-00125-a and by the Far East Branch of the Russian Academy of Sciences, project no. 12-I-P27-04.

REFERENCES

Bochkarev, V.S., Brekhuntsov, V.M., and Lukomskaya, K.G., On the Permian/Triassic rocks in western Siberia, *Gornye Vedomosti*, 2009, no. 2, pp. 7–17.

Chirkov, V.L., Gorbunov, I.N., Shadrina, S.V., et al., Geochemical and thermodynamic criteria for predicting the concentration of oil and gas in the basement of western Siberia, *Neftyanaya Promyshlennost'*, 2011, no. 4, pp. 41–45.

Efimov, V.A. and Sarafanova, L.A., Identification of fissure intervals in volcanogenic rocks based on general geological and geophysical data, in *Metody realizatsii potentsiala nefti i gaza v Khanty-Mansiiskom avtonomnom okruge–Yurga* (Methods for Realizing the Oil-and-Gas Potential in the Khanty-Mansi Autonomous Okrug–Yugra), vol. 2, 11th Industrial scientific conf., Khanty-Mansiisk: Izdat-NaukaServis, 2008, pp. 261–267.

Falta, R., Pruess, K., Finsterle, S., and Battistelli, A., *T2VOC User's Guide, Report LBNL-36400*, Berkeley, CA, US, 1995.

Finsterle, S., *iTOUGH2 User's Guide*, Report LBNL-40040, Berkeley, Ca, US, 1999.

Kireeva, T.A., The genesis of ground water in the White Tiger, Vietnam oil field in relation to the distribution of oil and gas, *Vestnik MGU, Ser. 4, Geologiya*, 2010, no. 4, pp. 35–40.

Kiryukhin, A.V., Modeling studies: the Dachny geothermal reservoir, Kamchatka, Russia, *Geothermics*, 1996, vol. 25, no. 1, pp. 63–90.

Kiryukhin, V.A., *Regional'naya gidrogeologiya* (Regional Hydrogeology), St. Petersburg: Sankt-Peterburgskii Gornyi Institut, 2005.

Kiryukhin, A.V., Nikolaeva, E.V., and Baturin, A.Yu., Comparative analysis of geologic–thermodynamic models of oil and thermal fields, in *Materialy Vserossiiskoi konferentsii "Degazatsiya Zemli: geodinamika, geoflyuidy, gaz i ikh paragenezy"* (Proc. All-Russia conf. Degassing of the Earth: Geodynamics, Geofluids, Gas and Their Parageneses), Moscow: GEOS, 2008, pp. 204–206.

Kiryukhin, A.V., Kiryukhin, V.A., and Manukhin, Yu.F., *Gidrogeologiya vulkanogenov* (Hydrogeology of Volcanic Rocks), St. Petersburg: Nauka, 2010.

Kiryukhin, A.V., Polyakov, A.Y., and Mushinsky, A.V., Inverse modeling of laboratory tests for rock thermal property estimation, in *Proc. Thirty-Seventh Workshop on Geothermal Reservoir Engineering*, Stanford University, Stanford, California, January 30–February 1, 2012, SGR-TR-194, pp. 446–451.

Kiryukhin, A.V., Xu, T., Pruess, K., et al., Thermal–hydrodynamic–chemical (THC) modeling based on geothermal field data, *Geothermics*, 2004, vol. 33, no. 3, pp. 349–381.

Kiryukhin, A.V., Comparative analysis of the structural hydrogeological conditions of the high temperature geothermal reservoirs and oil deposit in volcanic areas, in *Proc. World Geothermal Congress*, 2010, Bali, Indonesia, 2010, pp. 5.

Korovina, T.A., Kropotova, E.P., Minchenkov, N.N., et al., Pre-Jurassic basement in western Siberia—A new insight into a natural object of oil and gas distribution: A study of the Rogozhnikovskii reservoir, in *Metody realizatsii potentsiala nefti i gaza v Khanty-Mansiiskom avtonomnom okruge–Yurga* (Methods for Realizing the Oil-and-Gas Potential in the Khanty-Mansi Autonomous Okrug–Yugra), vol. 1, 12th Industrial scientific conf., Khanty-Mansiisk: Izdat-NaukaServis, 2009, pp. 214–218.

Korovina, T.A., Kropotova, E.P., and Braduchan, Yu.V., Absolute and stratigraphic dating of pre-Jurassic volcanogenic rocks based on isotope and palinologic studies in the Rogozhnikovskii area, in *Problemy geologii, bureniya i razvitiya neftyanykh i gazovykh polei v Surgutskom regione* (Problems in the Geology, Drilling, and Development of Oil and Gas Fields in the Surgut Region), vol. 10, Moscow: Neftyanoe Khozyaistvo, 2010, pp. 100–108.

Korzhinskii, D.S., *Teoriya metasomaticheskoi zonal'nosti* (A Theory of Metasomatic Zonality), Moscow: Nauka, 1982.

Matusevich, V.M., Ryl'kov, A.V., and Ushatinskii, I.N., *Geoflyuidal'nye sistemy i problemy neftegazonosnosti Zapadno-Sibirskogo megabasseina* (Geofluid Systems and Problems of Oil-and-Gas Potential in the Western Siberian Megabasin), Tyumen', TGNU, 2005.

Pruess, K., Two-phase unsaturated flow at Yucca Mountain, Nevada: A report on current understanding, *Flow and Transport Through Unsaturated Fractured Rock*, 2nd Ed., AGU Geophys. Monogr. 42, 2001, pp. 113–133.

Pruess, K., Oldenburg, C., and Moridis, G., *TOUGH2 User's Guide, Version 2.0, Report LBNL-43134*, Berkeley: CA, US, 1999.

Shadrina, S.V., Volcanic rocks of the Rogozhnikovskii reservoir (western part of the western Siberian geosyncline), in *Vserossiiskaya nauchnaya konferentsiya* (All-Union Science Conference), Tomsk, 2009, pp. 325–328.

Shadrina, S.V. and Smirnova, E.V., The volcanogenic complex of the Rogozhnikovskii area, in *Vserossiiskaya nauchnaya konferentsiya "Fundament i struktura Zapadno-Sibirskogo mesozoisko-kainozoiskogo osadochnogo basseina, geodinamicheskaya evolyutsiya i problemy nefti i gaza" (All-Russia science conference "The Basement and Structure of the Western Siberian Mesozoic–Cenozoic Sedimentary Basin, Geodynamic Evolution and Problems of Oil and Gas")*, Tyumen'–Novosibirsk, 2008, pp. 231–234.

Slovtsov, I.B., Rock alteration in the Mutnovsky hydrothermal system, Kamchatka, Russia, *Proc. of Water-Rock Interaction X*, July 10–15, 2001, Villasimius, Italy, Cidu, R., Ed., Balkema Swets & Zeitlinger, Lisse, 2001, pp. 915–918.

Xu, T., Sonnenthal, E., Spycher, N., and Pruess, K., *TOUGHREACT User's Guide: A simulation program for nonisothermal multiphase reactive geochemical transport in variably saturated geologic media*, LBNL-55460, 2006.

Translated by A. Petrosyan